

Article

Assessment of the Maize Crop Water Stress Index (CWSI) Using Drone-Acquired Data Across Different Phenological Stages

Mpho Kapari ^{1,*} , Mbulisi Sibanda ¹ , James Magidi ² , Tafadzwanashe Mabhaudhi ^{3,4,5} ,
Sylvester Mpandeli ^{6,7,8} and Luxon Nhamo ^{4,6,*} 

- ¹ Environmental Studies & Tourism, Faculty of Arts, Department of Geography, University of the Western Cape, Bellville, Cape Town 7535, South Africa; msibanda@uwc.ac.za
 - ² Geomatics Department, Tshwane University of Technology, Pretoria 0001, South Africa; magidijt@tut.ac.za
 - ³ Centre on Climate Change and Planetary Health, London School of Hygiene and Tropical Medicine (LSHTM), London WC1E 7HT, UK; tafadzwanashe.mabhaudhi@lshtm.ac.uk
 - ⁴ Centre for Transformative Agricultural and Food Systems (CTAFS), School of Agricultural, Earth and Environmental Sciences, University of KwaZulu-Natal, Pietermaritzburg 3209, South Africa
 - ⁵ United Nations University Institute for Water, Environment and Health, Richmond Hill, ON 225, Canada
 - ⁶ Water Research Commission of South Africa, Lynwood Manor, Pretoria 0081, South Africa; sylvesterm@wrc.org.za
 - ⁷ Department of Environmental, Water and Earth Sciences, Tshwane University of Technology, Pretoria 0029, South Africa
 - ⁸ Faculty of Science, Engineering and Agriculture, University of Venda, Thohoyandou 0950, South Africa
- * Correspondence: 4280223@myuwc.ac.za (M.K.); luxonn@wrc.org.za (L.N.)

Abstract: The temperature-based crop water stress index (CWSI) is the most robust metric among precise techniques that assess the severity of crop water stress, particularly in susceptible crops like maize. This study used a unmanned aerial vehicle (UAV) to remotely collect data, to use in combination with the random forest regression algorithm to detect the maize CWSI in smallholder croplands. This study sought to predict a foliar temperature-derived maize CWSI as a proxy for crop water stress using UAV-acquired spectral variables together with random forest regression throughout the vegetative and reproductive growth stages. The CWSI was derived after computing the non-water-stress baseline (NWSB) and non-transpiration baseline (NTB) using the field-measured canopy temperature, air temperature, and humidity data during the vegetative growth stages (V5, V10, and V14) and the reproductive growth stage (R1 stage). The results showed that the CWSI (CWSI < 0.3) could be estimated to an R^2 of 0.86, RMSE of 0.12, and MAE of 0.10 for the 5th vegetative stage; an R^2 of 0.85, RMSE of 0.03, and MAE of 0.02 for the 10th vegetative stage; an R^2 of 0.85, RMSE of 0.05, and MAE of 0.04 for the 14th vegetative stage; and an R^2 of 0.82, RMSE of 0.09, and MAE of 0.08 for the 1st reproductive stage. The Red, RedEdge, NIR, and TIR UAV-bands and their associated indices (CCCI, MTCI, GNDVI, NDRE, Red, TIR) were the most influential variables across all the growth stages. The vegetative V10 stage exhibited the most optimal prediction accuracies (RMSE = 0.03, MAE = 0.02), with the Red band being the most influential predictor variable. Unmanned aerial vehicles are essential for collecting data on the small and fragmented croplands predominant in southern Africa. The procedure facilitates determining crop water stress at different phenological stages to develop timeous response interventions, acting as an early warning system for crops.



Academic Editor: Adrian Marius Deaconu

Received: 17 January 2025

Revised: 3 March 2025

Accepted: 4 March 2025

Published: 6 March 2025

Citation: Kapari, M.; Sibanda, M.; Magidi, J.; Mabhaudhi, T.; Mpandeli, S.; Nhamo, L. Assessment of the Maize Crop Water Stress Index (CWSI) Using Drone-Acquired Data Across Different Phenological Stages. *Drones* **2025**, *9*, 192. <https://doi.org/10.3390/drones9030192>

Copyright: © 2025 by the authors. Licensee MDPI, Basel, Switzerland. This article is an open access article distributed under the terms and conditions of the Creative Commons Attribution (CC BY) license (<https://creativecommons.org/licenses/by/4.0/>).

Keywords: crop early warning; random forest classifier; smallholder farming; food security; resilience and adaptation; remote sensing

1. Introduction

Agricultural production in sub-Saharan Africa has been at risk due to the increasing water scarcity challenges compounded by erratic weather patterns and global warming [1]. In South Africa, smallholder farming consists of plots smaller than two hectares, which mainly depend on highly variable and unreliable rainfall [2]. As such, researchers are focusing on developing new crop varieties capable of withstanding local harsh climatic conditions. Maize (*Zea mays* L.) is a multi-systemic crop whose specific varieties can be adapted to suit any weather conditions [3]. Currently, it is a basic crop for the vulnerable, and it contributes to global food security [4]. Nonetheless, the foremost environmental challenge that hinders the production of maize is water stress [5]. Water stress affects maize crops at different stages, thereby impacting both the vegetative and reproductive growth of the crop [5].

Maize requires more water during the reproductive stage [6]. Consequently, maize yield can be significantly reduced due to water stress during the vegetative and reproductive growth stages. The authors of [7] demonstrated that water stress during rapid vegetative growth led to up to 40% grain yield loss, which was indicated physiologically by a reduction in plant extension and a drop in leaf size. Similarly, the authors of [8] noted that water scarcity resulted in a decrease in leaf growth rates, leaf numbers, leaf area, and plant height, which ultimately led to significant losses in terms of crop production. In this regard, there is an urgent need to exert efforts towards detecting and understanding the tolerance of crops to abiotic stresses. This is particularly true for rainfed agriculture in countries receiving less than 500 mm of precipitation, as this amount is below the critical levels required for obtaining good yields [3]. Therefore, it is necessary to determine water stress levels in maize crop fields at different crop developmental stages to implement appropriate response measures and mitigate their impacts on crop production.

In the assessment of crop water stress, researchers have utilized different thermal indices over the last few decades. The canopy–air temperature difference (CATD) was used as an indicator of crop water stress in the work by [9]. They introduced the concept of “stress degree day (SDD)”, which is defined as the cumulative difference between canopy and air temperatures during mid-afternoon over a specified duration [9]. Ref. [10] emphasized the effective and non-invasive utilization of CATD for quickly monitoring the overall plant response to water stress. Furthermore, the authors of [11] presented a method for assessing plant water status relative to the temperature difference between a well-watered crop and a stressed crop. They termed this temperature difference as the “temperature stress day” (TSD). The authors of [12] implemented the “temperature–time threshold” (TTT) irrigation management system, where the canopy temperature surpasses the threshold temperature every minute, and the cumulative value of TTT is calculated. The variables based on canopy temperatures, such as CATD, SDD, or TSD, standardize canopy temperature in relation to air temperature. However, the evapotranspiration demand, which significantly influences water stress in crop plants, is largely controlled by the vapour pressure deficit of the surrounding air [13].

The sensitivity of the canopy temperature (T_c) to changing weather conditions resulted in the development of the crop water stress index (CWSI) [14], which accounts for the impact of air temperature (T_a) and other meteorological factors, such as the vapour pressure deficit (VPD), wind speed (WS), and relative humidity (RH) [15], thus making it more suitable for water stress measurement [16]. The CWSI measures crop water stress based on canopy temperature and, therefore, reduces the need for ground surveys [17]. There are two widely used CWSI models: the theoretical model [15] and the empirical model [9]. The primary benefit of the empirical approach is attributed to the fact that it is relatively cheap, and its implementation only necessitates the measurement of three variables: canopy temperature,

relative humidity, and vapour pressure deficit (T_a , RH, and VPD, respectively) [16,17]. The empirical approach utilizes the relationship between the disparity in canopy temperature and air temperature ($T_c - T_a$), along with the vapour pressure deficit of the atmosphere (VPD), in both water-stressed and non-water-stressed conditions [18]. The lower limit baseline is formed by the linear relationship between the $T_c - T_a$ and VPD values for well-irrigated plants, and at the given VPD, the upper baseline is created by the $T_c - T_a$ values of water-stressed plants [19,20]. As such, the CWSI has been the most commonly used index for assessing crop water stress by examining the canopy temperature [21].

The computation of the CWSI has been explored as an effective method for monitoring the crop water status for maize [22,23]. However, the aforementioned studies that utilized the CWSI to assess crop water stress used point-based approaches that did not take into consideration the spatial variability in crops. Other than the application of fine spatial resolution UAV-acquired images, the integration of robust machine learning algorithms and vegetation indices (VIs) in predicting crop water stress indicators has shown to be effective in mapping crop water stress in a spatially explicit manner (Zhao et al., 2018). In the quantification of water stress in plants, numerous VIs have been identified that are particularly useful for both direct and indirect quantification [24,25]. Such indices include the renormalized difference vegetation index (RDVI), normalized difference vegetation index (NDVI), soil-adjusted vegetation index (SAVI), transformed chlorophyll absorption in reflectance index (TCARI), and optimization of soil-adjusted vegetation index (OSAVI), which are based on visible, near-infrared (NIR), and RedEdge bands [25]. These VIs are significant in providing vital vegetation information because of their sensitivity to vegetation density and biomass (e.g., NDVI and SAVI), as well as leaf water content (e.g., NDWI) [26]. These VIs are used to monitor and predict leaf area, leaf chlorophyll absorption, and crop water stress, as well as for other applications. However, when these indices are used to predict crop characteristics, they are influenced by the soil background; to reduce this impact, indices including TCARI/OSAVI are used [27]. The use of machine learning techniques has been encouraged because they can predict trends and accurately anticipate major crop parameters in the multitemporal collection of many spectral bands and VIs, generating highly dimensional data [28].

In particular, a commonly used machine learning algorithm is the random forest (RF), which operates by obtaining predicted values from combined decision trees [29]. Compared to other machine learning algorithms, the RF is easy to execute, is more robust, and has been known to be resistant to overfitting issues [29,30]. Moreover, the RF model is a non-linear method that provides high simulation accuracy as well as an easy model development process [31]. It is nonparametric and well-known for its capacity to detect subtle differences in multiple spectral variables without being affected by collinearity, variable autocorrelation, or model overfitting [32]. Moreover, the RF offers the benefit of employing a bootstrapping mechanism that optimizes resampling and data utilization when drawing training data points to build trees for each model, irrespective of the sample size [32]. The RF has been extensively used for crop monitoring because of its rapid computational speed, as well as its good degree of stability in comparison with linear regression and Neural Network algorithms [33]. The RF may consider multiple variables, is highly stable with changes in the parameter values of a classification model, and can average tree forecasts for each forest.

As a result, in terms of classification and prediction, the RF has an advantage. Therefore, the RF was expected to be a suitable method for precisely estimating leaf temperature and stomatal conductance as signs of crop water stress in small-scale farms. The RF regression algorithm was used to predict the maize CWSI from spectral bands and VIs because it can develop a multicollinear and multidimensional analysis on large databases [32]. Given

the possibilities presented by UAV data and machine learning techniques in evaluating crop water stress, this research examined the practicality of using UAVs to determine the CWSI for maize crops. The random forest algorithm was used to assess the maize CWSI in a smallholder farm across different phenological stages, from the vegetative to reproductive stages, and determine the optimal stage to deduce the CWSI. The objectives were to determine maize water stress using the crop water stress index (CWSI) for the various maize phenological stages and estimate the optimal maize growth stage(s) for crop water stress index (CWSI) model prediction.

2. Materials and Methods

2.1. Description of the Study Area

This research was conducted on a 0.28-hectare smallholder maize field (Figure 1). This study field (-22.125031° to -34.834171° S and 16.451891° to 32.891122° E) is situated 55 km to the northeast of Pietermaritzburg, within the rural region of Swayimane, uMshwathi Local Municipality, in the KwaZulu-Natal Province of South Africa (Figure 1). The area is dominated by smallholder farming systems, which are mainly rainfed. The main crops grown in the region consist of maize, sugarcane, sweet potato, and amadumbe (taro). Here, smallholder farmers use traditional agricultural techniques to plant, care for, and manually harvest their crops. Farm plots rely on natural rainfall for irrigation and are fertilized with animal manure, as well as manually weeded by farmers. As an alternative, small-scale farmers utilize herbicide backpack sprayers to manage weeds and grasses.

Furthermore, crop production in the area thrives due to the favourable environmental conditions in the region, where summers are mainly warm and wet, whilst winters are dry. The yearly temperatures vary from 11.8°C to 24°C , with an average annual temperature of 17°C . The annual precipitation ranges from 600 mm to 1200 mm, with the majority of rainfall occurring during the summer months. The area experienced an average humidity of 82.81%, 242.8 mm rainfall, and the highest air temperature of 24°C over the study period [34]. An automated weather station located at Swayimane Primary School, approximately 2 km away from the maize field, kept track of the weather conditions.

2.2. Methodological Framework

Figure 2 is a flowchart of activities undertaken to assess the maize CWSI using machine learning algorithms and the derivation of the results. This work included data collection, as represented by the blue colour, data preparation, application, and analysis using machine learning algorithms (the random forest), as shown by the orange colour, and, lastly, data analysis and the derivation of results, as shown by the activities indicated in the green colour (Figure 2). The stages of the flowchart were repeated at every phenological phase of the maize crop. Each of these stages is detailed in the preceding sub-sections.

2.3. Maize Phenotyping

The maize seeds were sown on 8 February and harvested on 26 May 2021, resulting in a total growth period of 108 days. Maize development is divided into vegetative stages and reproductive stages, as outlined by [7]. Within each stage, maize growth and development encounter certain transitions as a function of the environmental conditions under which it is grown, as well as the crop's genetic potential. These are significant to deduce for monitoring and informing smallholder farmers so that the farmers can manipulate the growth environment at the right time to increase yields. Although these stages are outlined in the work by [35], Table 1 only outlines stages that were examined for this study. These stages were chosen due to data availability as well as their significant characteristics in maize growth and development.

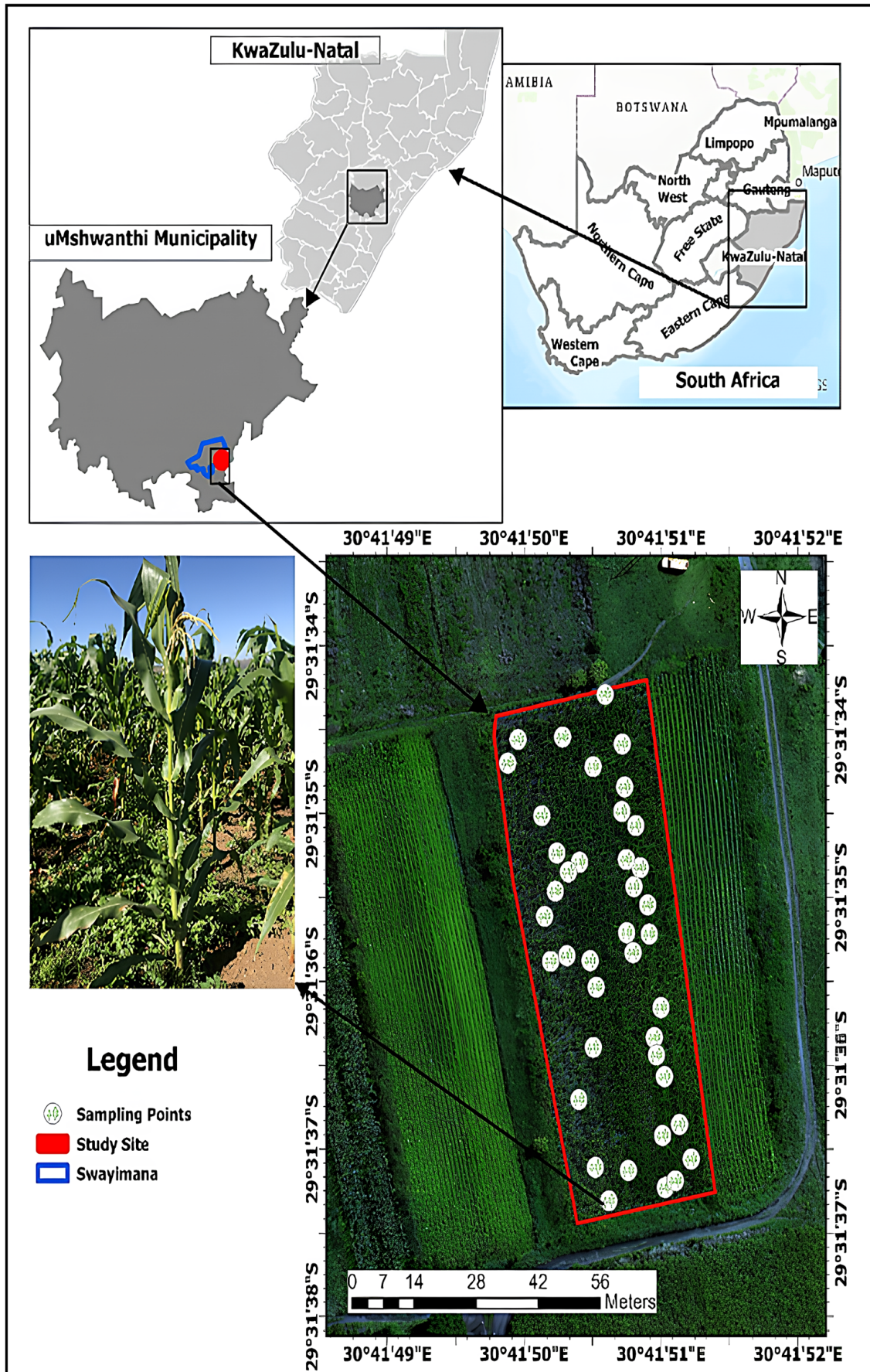


Figure 1. Location of the Swayimane study area, study site, and smallholder maize field.

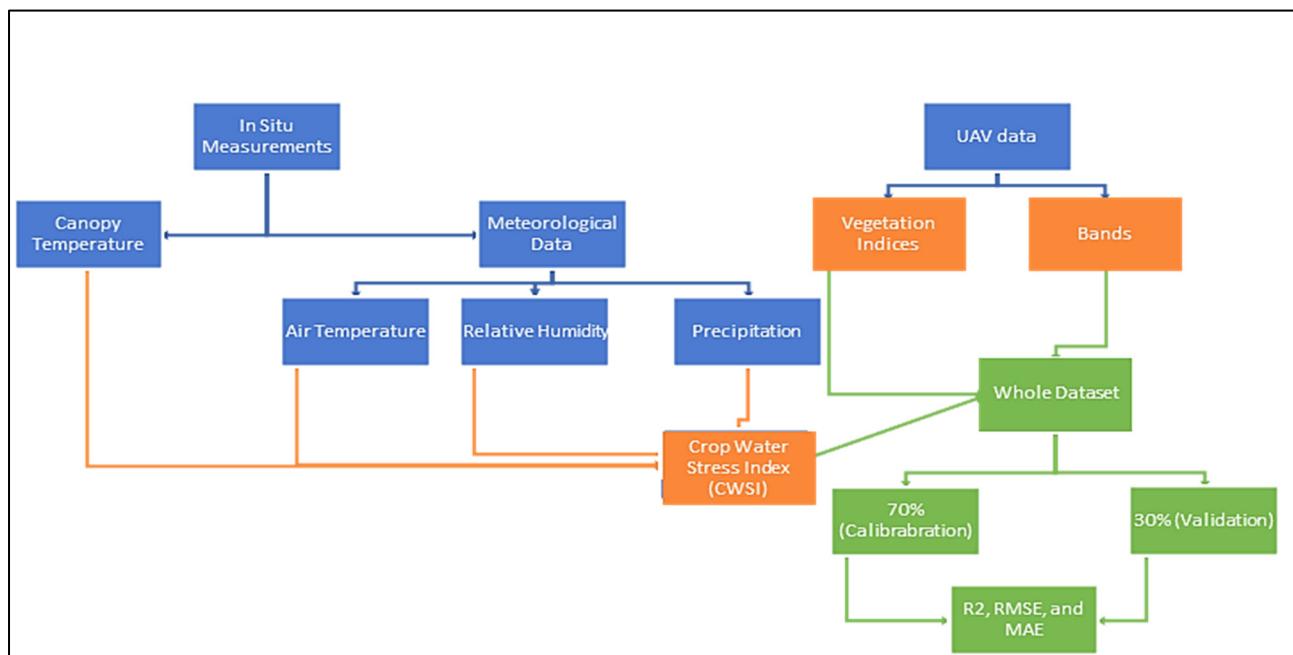






Figure 2. Flowchart showing the data collection (blue), data preparation RF analysis (orange), and data analysis (green).

Table 1. Assessed maize growth stages and their characteristics.

Days After Emergence	Growth Stage	Description	Pictures
21–31	V5	The plant population is established at this stage as potential cobs and tassel forms. Thus, the yield potential is determined. A growth point of 20 to 25 mm below the surface.	
38–43	V10	Early cob development and ear initiation.	
49–55	V14	Tassel begins to grow fast at the growth point. From the sixth to the eighth node above the surface, active development of lateral shoots and cobs. Brace root development. Highly sensitive to heat and drought stress; thus, farmers should avoid any nutrient and water shortages to ensure maximum cob and kernel development.	
63–69	R1	Pollination takes over for a 5–10-day period. Maize is sensitive to stress during this period; thus, if leaves are already wilted from moisture stress in the morning, a crop loss of about 7% per day is experienced. Maize begins to translocate nutrients from other parts of the plant to the cob.	

Vegetative stages.

Reproductive stage.

2.4. Maize Canopy Temperature Measurement

The canopy temperature was recorded with two infrared radiometers (IRRs) (Apogee SI-111, Apogee Instruments Inc., Logan, UT, USA) situated on a four-meter meteorological tower at the centre of the maize field (Figure 3). The temperature measurement readings from these sensors ranged from $-60\text{ }^{\circ}\text{C}$ to $110\text{ }^{\circ}\text{C}$ in the $8\text{--}14\text{ }\mu\text{m}$ range. Additionally, the field of view (FOV) was set at a 23° and 45° half-angle perpendicular to the row direction to obtain canopy temperature data. The canopy temperature was obtained every 10 s and then later averaged to 5, 10, 30, and 60 min using a datalogger CR1000 (Campbell Scientific, Logan Utah, USA) (Figure 3). This study used 60 min interval foliar temperature data to develop the non-water-stressed baseline (NWSB) and non-transpiring baseline (NTB) for the vegetative and reproductive stages.

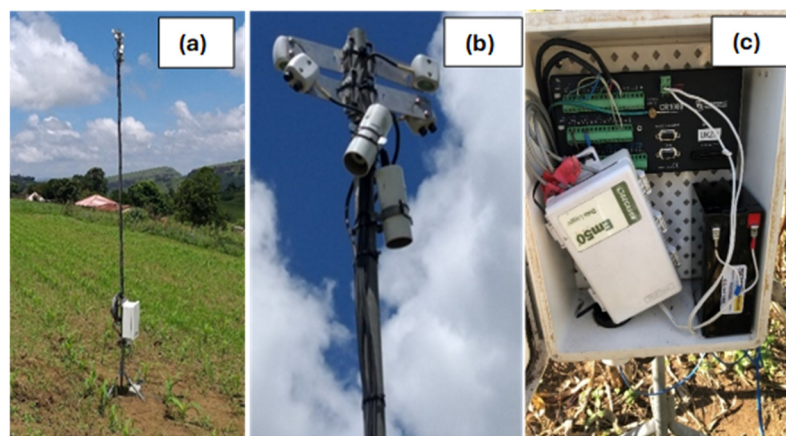


Figure 3. (a) An automated in-field meteorological tower in the maize field, (b) meteorological tower-mounted infrared radiometers (IRRs), and (c) a CR1000 data logger, an Em50 datalogger, and a 12 V battery.

The calibration of the IRR sensors was conducted by a chamber that is temperature-controlled with blackbody cones for radiation sources, where the sensors were held at an opening on the blackbody. Thermal isolation from the cones was used for each of the IRR sensors, which were monitored at their respective temperatures. The IRR was kept at a steady temperature, while the cone was regulated to temperatures below $12\text{ }^{\circ}\text{C}$, above $18\text{ }^{\circ}\text{C}$, and consistent with the IRR. For every $10\text{ }^{\circ}\text{C}$ measured, measurements of IRR and black body cones were performed until they reached at least a constant temperature. The IRR measurements and the maize temperature-calibrated handheld IRT measurements were used for the development of the CWSI.

The experimental field polygon was digitized using Google Earth Pro and thereafter used in ArcGIS 10.5 for generating sampling points. To obtain a total of 50 sample points within the digitized field perimeter, systematic random sampling was then conducted. The coordinates were then transferred to the handheld GPS unit of Trimble Global Positioning System with submeter accuracy. To navigate the sampling zones, these locations were used. A maize plant situated near the sampling location was chosen and evaluated for this study upon reaching the sampling point. Maize plants at each sampling site were marked in order to achieve consistency with the measurements completed once a week. A handheld infrared GM320 thermometer (IRT) with digital laser was used to measure foliar temperature data during the early vegetative growth to late reproductive growth stages of maize at two-week intervals.

Temperature measurements were recorded at each sampling point/plant from 10:00 a.m. to 14:00 p.m. (South Africa Standard Time). Temperature measurements of the maize canopy were captured simultaneously with the image acquisition using the

drone across all field sampling dates. Foliar (IRT-measured) temperature readings were conducted from a fresh, completely visible ear of the leaf with the collar visible during the vegetative stage. Thereafter, the foliar temperature was then measured from the ear leaf [32]. Temperature measurements from IRT were conducted and averaged three further times. Each temperature measurement was then captured in a spreadsheet, along with other measured crop properties, including stomatal conductance. The SC-1 leaf porometer (Decagon Devices, Inc., Pullman, WA, USA) was used to measure stomatal conductance in $\text{mmol m}^{-2} \text{s}^{-1}$ for a period of 30 s. The multispectral and thermal UAV imagery was combined with all the field-measured samples to create a point map.

2.5. Meteorological Data Collection

The automatic weather stations (AWSs) set up at Swayimane Primary School, following the World Meteorological Organization's guidelines, were utilized to gather meteorological data [32]. Hourly averaged meteorological information, such as relative humidity (%) and air temperature ($^{\circ}\text{C}$), was employed to calculate the vapour pressure deficit (VPD) for determining NWSB and, ultimately, the CWSI.

2.6. UAV Multispectral-Thermal System

A quad-rotor UAV, specifically, the DJI Matrice 300 (DJI Inc., Shenzhen, China), along with a Micasense (MicaSense, Inc., Seattle, WA, USA) multispectral sensor system, was employed to gather images for this research (Figure 3b). The camera system was characterized by a Downwelling Light Sensor 2 (DLS-2) integrated with a GPS module (RedEdge, MicaSense Inc., Seattle, WA, USA) that records high-resolution five-band multispectral narrow bands (blue, green, red, red-edge, near-infrared (NIR)) (Table 2), along with a longwave infrared thermal camera that meets the specifications in [32,36].

Table 2. MicaSense Altum camera specifications.

Band	Spectral Colour	Band Range	Ground Sampling Distance at a Flying Height of 120 m
1	Blue	475 nm	5.2 cm per pixel
2	Green	560 nm	5.2 cm per pixel
3	Red	668 nm	5.2 cm per pixel
4	Red-edge	717 nm	5.2 cm per pixel
5	Near-infrared	842 nm	5.2 cm per pixel
6	Thermal infrared	8000–14,000 nm	81 cm per pixel

2.7. Image Acquisition and Processing

The flight plan was designed using field boundary digitized on Google Earth Pro and integrated into the UAV's smart interface in a keyhole markup language format (kml) (Figure 4c). A flight controller was used to generate a flight plan, which the aircraft traced while capturing the images. After the flight plan's generation, the flight-specific details were obtained, as illustrated in Table 3. Prior to image acquisition, the MicaSense Altum calibrating reflectance panel (CRP) was utilized to adjust the sensor prior to and following the flight (Figure 4d). This involved the pilot directly capturing an unshaded image above the CRP to assess the lighting conditions before and after the flight. The remotely acquired dataset was acquired using the UAV at 2-week intervals and simultaneously with the other crop elements.

Once the images were gathered, they were combined into a mosaic and adjusted for radiometric accuracy using Pix4Dfields software (Pix4d Inc., San Francisco, CA, USA). Images from the CRP acquired before and after the acquisition of the flights were used to calibrate the capture reflectance values from possible variabilities imposed by changes

in atmospheric conditions. A complete orthomosaic GeoTiff image was generated after pre-processing. Reference points selected in Google Earth Pro were utilized to orthorectify the image in ArcGIS 10.5. The images were aligned to the Universal Transverse Mercator (UTM zone 36S) projection, achieving a root mean square error (RMSE) of less than 0.5 pixels (3.5 cm).

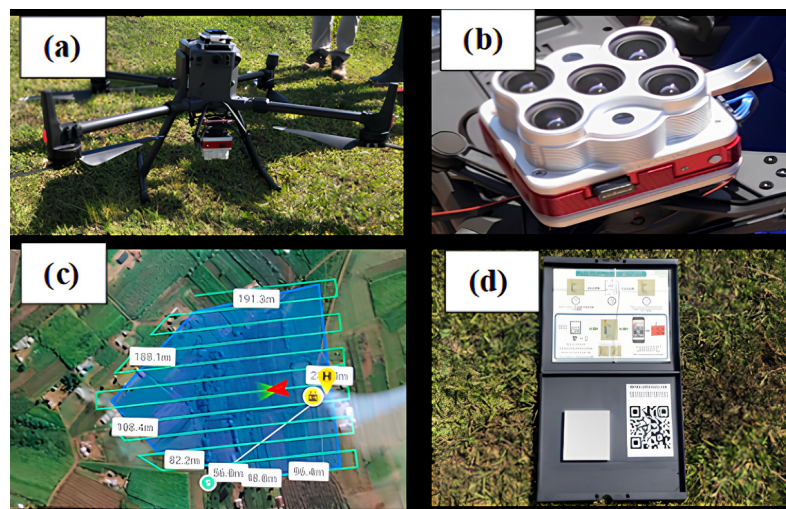


Figure 4. (a) UAV system, DJI Matrice 300, (b) MicaSense Altum camera, (c) DJI M-300 flight plan, and (d) MicaSense Altum calibration reflectance panel.

Table 3. Unmanned aerial vehicle (UAV) flight specifications.

Parameters	Specifications
Altitude	100 m
Ground sampling distance (multispectral)	7 cm
Ground sampling distance (thermal infrared)	109 cm
Speed	16 m/s
Flight duration	14 min 36 s
Composite images	321
Image overlap	80%

2.8. Selection of Vegetation Indices

The temperature readings depicted on the point map, as described in Section 2.7, were utilized to obtain reflectance values for the multispectral bands. These surface reflectance values were subsequently applied to calculate vegetation indices. The chosen vegetation indices are well-established for correlating with canopy physiological parameters [37]. Furthermore, these indices seek to enhance the role of vegetation optical traits in the overall spectral response of the canopy [37]. The vegetation indices also attempt to correct any confounding factors, such as soil bottom reflectivity in the crop, especially in the early stages of the growth cycle [38]. To create a regression model that links data collected by UAVs with the CWSI, incorporating multispectral and thermal bands, along with Vis in the work by [34], were selected.

2.9. Crop Water Stress Index (CWSI) Calculation

The CWSI was calculated by using Equations (1)–(3):

$$CWSI = \frac{\Delta T - T_{wet}}{T_{dry} - T_{wet}} \tag{1}$$

where ΔT is the precise calculation of the disparity between canopy and air temperature ($T_c - T_a$), T_{wet} as the lower boundary, and T_{dry} as the upper boundary for the predicted

baselines. In this context, T_{wet} and T_{dry} are also known as the non-water-stressed baseline (NWSB) and the non-transpiring baseline (NTB), respectively, which are defined in the following manner:

$$T_{wet} = m * VPD + b \quad (2)$$

$$T_{dry} = m * VPG + b \quad (3)$$

where m and b in both equations represent the slope and intercept, respectively. VPD is obtained using Equations (4)–(6), as described in [39]:

$$e_s = 0.6108 * \exp\left[\frac{17.27T}{T + 237.3}\right] \quad (4)$$

$$e_a = e_s * \left(\frac{RH}{100}\right) \quad (5)$$

$$VPD = e_s - e_a \quad (6)$$

where T represents the air temperature, RH signifies the relative humidity, e_s denotes the saturated vapour pressure (kPa) at the air temperature T_a , and e_a is the actual vapour pressure (kPa). To compute T_{dry} values, the vapour pressure gradient (VPG) is calculated. The VPG represents the difference in air-saturated water vapour pressure at temperature T_a compared to the air-saturated water vapour pressure at temperature $T_a + b$ [40].

To begin with, the initial phase of calculating the CWSI consisted of establishing functions for T_{wet} and T_{dry} for rainfed maize based on the environmental conditions of Swayimane, as suggested in [41]. Maize ΔT was calculated by IRT measurements in the field after two significant rainfall days and was plotted with their corresponding VPD values. This was completed under the assumption that after these wetting events, the soil water deficit was replenished, and, therefore, maize had access to sufficient soil water. Therefore, non-water-stressed conditions existed. This was established for two hours prior to and two hours following noon, as suggested by [15]. The coefficients for Equations (5) and (6) were derived from the linear segment equation through the application of basic linear regression. To illustrate the correlation between ΔT and VPD during the vegetative and reproductive stages, a three-step moving average method was employed [9]. According to [41], the CWSI method is applicable solely in clear-sky situations; therefore, all the days chosen for calculating the CWSI aligned with the dates of field visits during all evaluated stages. The CWSI values span from 0 to 1, with 0 representing no water stress and 1 denoting the highest level of stress.

2.10. Statistical Analysis

RF regression was adopted in this study following its high performance in predicting the CWSI, surpassing SVM and partial least squares (PLS) [34]. The RF was implemented in RStudio software version 1.4.1564, and the outputs were a set of decision trees. Subsequently, the trees were divided at each node based on the explanatory variable that contributed most significantly to the response variable [42]. For every prediction of the response variable, an average value was generated from a variety of decision trees and their outputs. The models developed included spectral variables (bands and VIs) and the CWSI as the exploratory variable and response variable, respectively. Furthermore, all the models created for each stage of growth in this study have distinct hyperparameters that enhance their performance. In random forest (RF), the $mtry$ parameter represents the count of variables utilized to create splits at every node of the decision tree. In R, the standard value of $mtry$ is determined by taking the total number of predictive variables and dividing it by three [43]. Meanwhile, the other parameter, $ntree$, which indicates the generated number

of trees, has a default value of 500 [44]. This study employed the K-fold cross-validation method due to its noted effectiveness in the existing literature [45]. In this research, the complete process for developing the predictive model involved performing 10-fold cross-validation three times on the training dataset, utilizing the “train” function found in the “caret” package in R. This cross-validation approach allowed for the retention of the most effective components that achieved the lowest RMSE across all models. Ultimately, the final model for each phenological stage was optimized and fine-tuned with hyperparameters that included 500 trees and various VIs. Moreover, the final model was used to identify variables that were the most important for explaining the CWSI at each phenological stage using the “varImp” function in R. Thus, variable importance assessment was only applied on the optimal performing model at each stage. The dataset in this research was divided, with 70% allocated for training and 30% for testing purposes (Figure 4).

2.11. Accuracy Assessment

The effectiveness and reliability of the RF predictive models were evaluated using the coefficient of determination (R^2), the root mean square error (RMSE), and the mean absolute error (MAE).

3. Results

3.1. Non-Water-Stressed Baselines (NWSBs) and the Maize Crop Water Stress Index (CWS) for Vegetative and Reproductive Stages

Figure 4a,b show the correlation of $T_c - T_a$ vs. VPD, which was utilized to derive the slope and the intercept of the NWSB. The same coefficients developed for NWSB were also determined for NTB using VPG instead of VPD, while Figure 5 shows the significant correlation at the vegetative ($R^2 = 0.83$) and reproductive ($R^2 = 0.95$) stages. The results indicate that $T_c - T_a$ decreases when VPD increases.

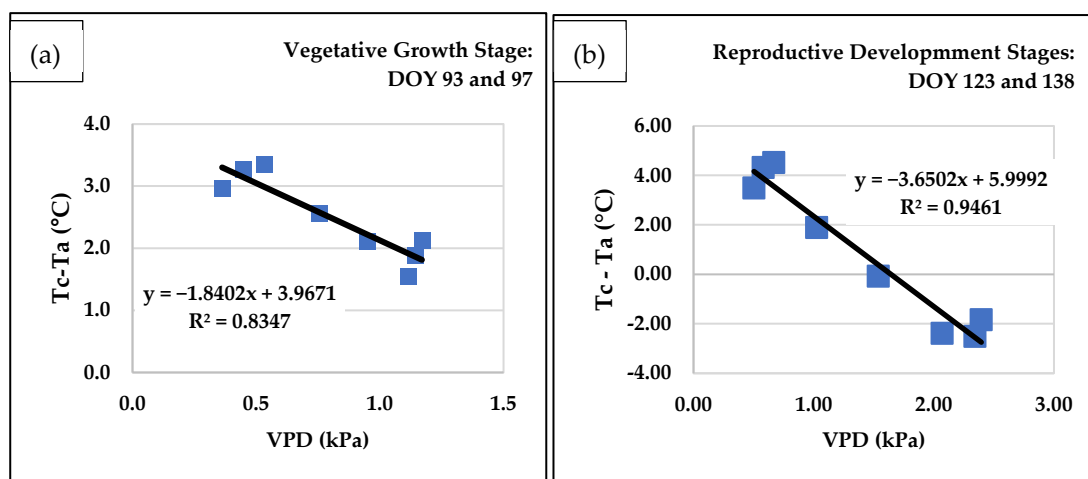


Figure 5. Non-water-stressed baselines used to calculate the CWSI for maize growth stages.

The trend in the CWSI for four distinctive days of the maize growth stages can be observed in Figure 5. The results show that the values of the CWSI are close to zero for the two growth stages. The lowest CWSI value was determined on DOY 76, whilst the highest value was determined on DOY 89. On average, there was low crop water stress during the study period. Generally, these findings show that maize water stress levels varied at different stages as maize grows from the vegetative to the reproductive stage. Figure 6 depicts that overall, for both stages, the maize incurred low water stress levels.

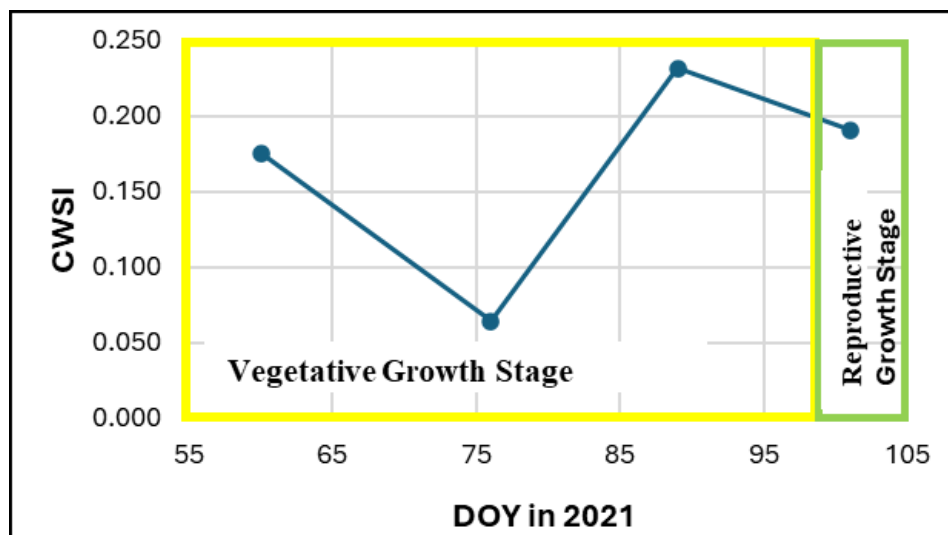


Figure 6. The variation in the CWSI for maize over different DOYs in 2021.

3.2. Predicting the Crop Water Stress Index (CWSI) of Maize During the Vegetative and Reproductive Growth Stages Using Random Forest

The CWSI was predicted at an RMSE of 0.12 and R^2 of 0.86 during the vegetative stage (V5) based on NDWI, SAVI, TCARI_RDVI, RedEdge, TIR, GNDVI, and MTCI (in order of importance) as optimal explanatory variables (Figure 7(ai,aii)). During the V10 growth stage, the CWSI was predicted at an RMSE value of 0.03 and an R^2 value of 0.85 using Red, TIR, GNDVI, TCARI, CI_GREEN, CCCI, and NIR, ranked by priority (Figure 7(bi,bii)). During the final vegetative stage (V14), the CWSI was predicted at an RMSE value of 0.05 as well as an R^2 of 0.85 using NDRE, MTCI, CCCI, GNDVI, TIR, CI_RedEdge, and MTVI2 as optimal variables, ranked by priority (Figure 7(ci,cii)). Meanwhile, during the reproductive stage, the CWSI of maize was estimated to have an RMSE of 0.09 and R^2 of 0.82 based on TIR, TCARI, RedEdge, Red, RDVI, RVI, and Green as the best variables, ranked by priority. Overall, the results indicate that the vegetation stage V10 was the optimal stage to predict the CWSI, with the lowest RMSE of 0.03 using Red, TIR, GNDVI, TCARI, etc., in that order. The least optimal stage to determine the CWSI was the early vegetative stage, with the highest RMSE of 0.12.

3.3. Spatial Distribution of the Maize Crop Water Stress Index (CWSI) at Different Phenological Stages

Figure 8 illustrates the spatial arrangement of the CWSI in the experimental field at different growth stages. The images (Figure 8) indicate that, on average, there were consistently low water stress levels throughout the stages. However, the CWSI increased as the maize grew and the phenological periods changed.

The early reproductive (R1) phenological period exhibited the highest CWSI, ranging from 0.05. Subsequently, the CWSI was minimal during the vegetative phase (V5, V10, and V14). Despite this, the results depicted in Figure 8 indicate that the western section of the field (Figure 8c,d) exhibited signs of water stress during the late vegetative phase and the early reproductive phase (V14 and R1). The observed outcomes can be attributed to the farmer's application of herbicides in the western section to eradicate the grass and weeds present between the rows during the mid-vegetative phase (V5 and V10). As a result, the herbicides negatively impacted the health of these crops, causing the plants to experience a slight herbicide burn and thus appear to have high stress. However, Tc-Ta increased as the winter season approached, suggesting reduced transpiration due to water stress during the mid-reproductive and senescence phases in the late reproductive growth stages.

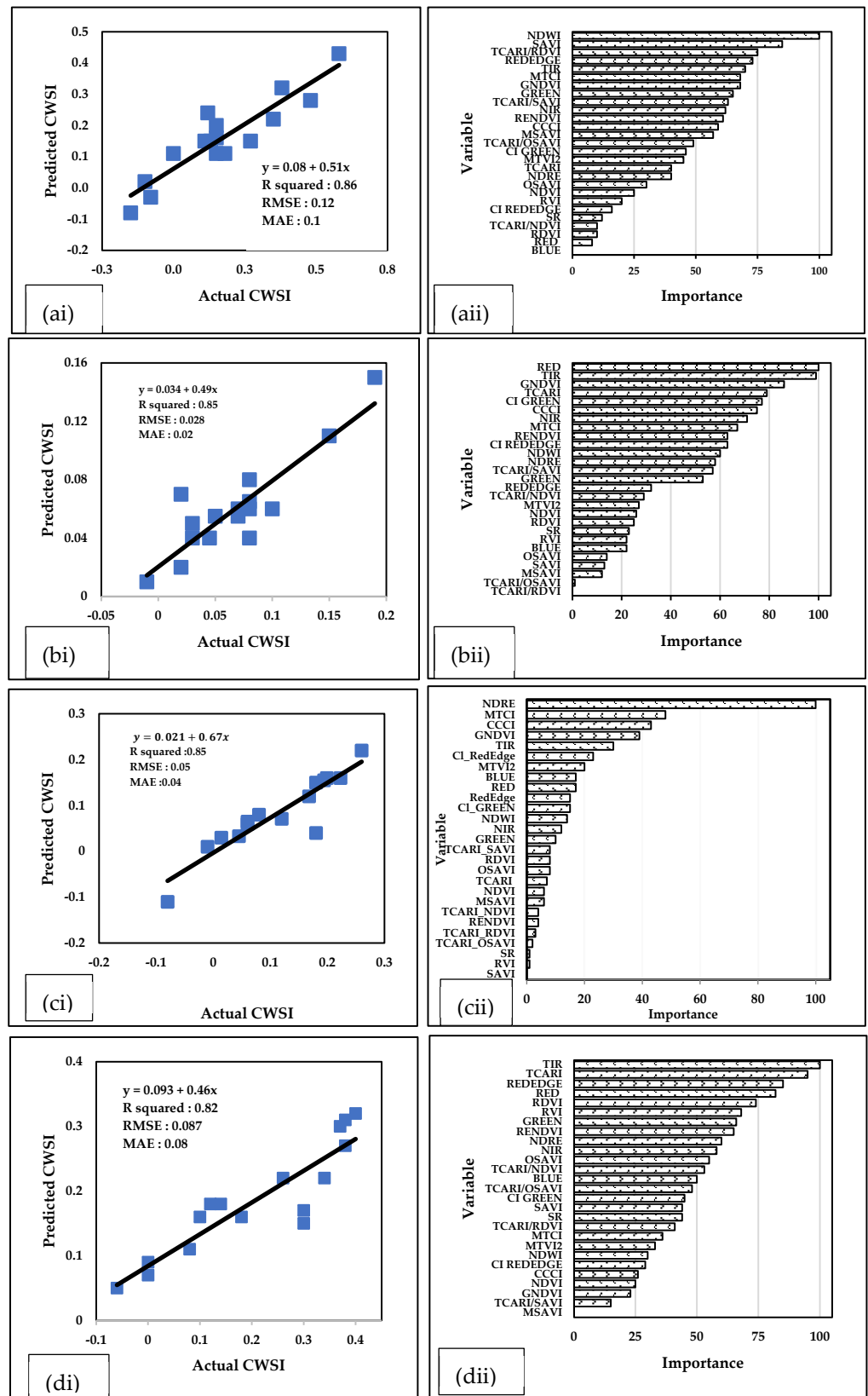


Figure 7. Linear relationships between the actual and predicted CWSI for maize crop’s vegetative stages (ai) V5, (bi) V10, and (ci) V14 and (di) reproductive stages (R1), as well as the corresponding variables’ importance (ai–dii).

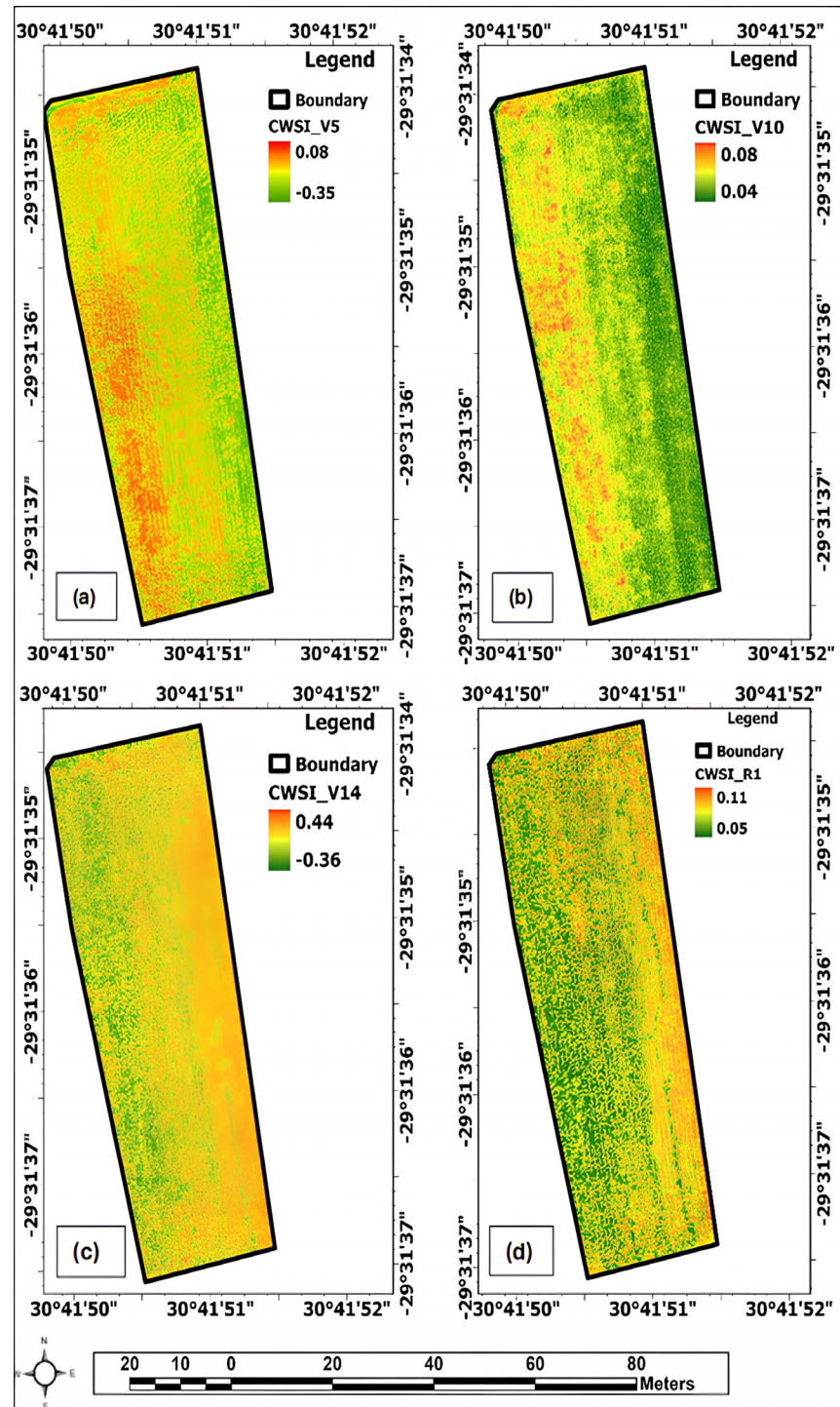


Figure 8. The maize CWSI over the smallholder field for vegetative stages (a–c) and reproductive stages (d).

4. Discussion

4.1. Determination of the Baselines and the Maize CWSI for the Vegetative and Reproductive Stages

According to the results, the NWSB slope during the reproductive stage was more pronounced than at the vegetative phase. Because the NWSB's gradient indicates the capacity for crop transpiration [40], the findings show that maize transpiration fluctuates based on alterations in microclimatic conditions at every stage (i.e., vegetative and reproductive growth stages). This leads to a T_c decrease due to growth from the vegetative to the reproductive stage, thus leading to a $T_c - T_a$ decrease and similar changes in VPD and,

concurrently, a decline in the NWSB slope. Additionally, this change in different stages can also be attributed to the change in the weather season from summer to winter as the maize stage changes from the vegetative stage to the reproductive stage. This is similar to the work performed by [46], who found that the baselines in different growth stages were related to variations in weather conditions from the beginning to the end of the growth stage, necessitating the need to determine baselines at each stage. Additionally, ref. [47] emphasized that there is a need to use different baselines to avoid a decline in the CWSI's ability to recognize variations under different water stress conditions. Consequently, when developing the CWSI empirical model, it was necessary to establish NWSB individually for various growth stages of maize.

Furthermore, the results also revealed that the intercept of NWSB in the vegetative stage was lower than in the reproductive stage, showing that as the maize continued to grow, the gap gradually increased. This further indicates that under the vegetative stage, the maize canopy temperature was lower than in the reproductive stage, and their T_c -s values were different. Similarly, various studies have found that there is a notable difference in the NWSB slope at different phenological stages. For instance, ref. [40] found that there is a significant difference in the NWSB slope of summer maize during jointing, the tasselling stage, milky ripening, and the maturity stage. This difference has also been noted in other crops. Ref. [48] found that the NWSB slope of greenhouse grapes was reduced in different stages, namely, the flowering, fruit swelling, and ripening stages at 3.56, 2.5, and 1.97, respectively. Additionally, ref. [49] found that the NWSB slope and intercept were significantly different for wheat in two consecutive stages; before and after heading, the slopes were -1.75 and -1.11 for both stages, respectively. This indicated that after heading, the slope of NWSB was less steep. Nonetheless, studies have reported slopes and intercepts ranging from -1.79 to 3.35 and 1.06 to 3.43 , respectively [17,41,50]. Our findings revealed that the slope and intercept values were not outside the range of the existing NWSB intercept and slope. This variability could be attributed to differences in climatic conditions, given that these values were determined under the Mediterranean climate, which differs from the tropical climate experienced in the KwaZulu-Natal province. To the best of our knowledge, maize baselines have not been identified in this region, resulting in a lack of literature for comparison.

The NWSB results were able to determine the CWSI for both the vegetative and reproductive stages. The results reveal that the CWSI was relatively low during these stages ($CWSI < 0.3$), which may well be because the study location received rainfall that could have replenished moisture in the soil, availing it for photosynthesis. Previous studies found that under well-irrigated conditions, CWSI values were less than 0.5 [17,51,52]. Notable results indicate that the CWSI values began to decline in the reproductive stage. Similarly, refs. [17,23] noted that the CWSI was lowest during the maize reproductive stage. Meanwhile, ref. [53] found that CWSI values over 0.40 led to a substantial reduction in yield. Adopting the CWSI as a water stress indicator is further recommended by [54–57], who suggested that, in comparison to techniques like soil moisture-based indicators, the CWSI provides a simpler indicator for detecting water stress.

4.2. Comparative Estimation of the CWSI in Maize Across Different Growth Stages

Based on the RF results, the V5 stage yielded the maximum RMSE of 0.12 using NDWI, SAVI, TCARI_RDVI, and RedEdge band as significant variables, in order of importance. These results indicate the CWSI's sensitivity to the RedEdge, Red, Green, and NIR bands, as well as their associated derivatives, as these indices were formulated using these spectral bands. This has been corroborated by the literature, which shows a statistically representative correlation between leaf reflectance across the spectrum and water quantity in crop

leaves [58]. Specifically, the RedEdge section has been related to crop water stress [55,59]. This is due to RedEdge's capability to record the changes in chemical and physiological processes generated by photosynthetic activities, stomatal conductance, and crop foliar temperature [24]. Additionally, because of its sensitivity to high foliar reflectance due to pigment concentrations within plants' canopy structure, the Red and NIR regions have been largely related to the chlorophyll concentration [60,61]. Red, RedEdge, and NIR bands and the associated VI significance in this early vegetative stage indicates strong chlorophyll concentrations due to low leaf area values, leading to a higher dynamic crop photosynthesis rate and enabling high reflectance in RedEdge and NIR sections [62]. Furthermore, in the V5 stage, the NDWI was able to explain the variations in the maize CWSI, owing to its strong correlation with plant water stress [40]. However, since the NDWI was developed to monitor crop water stress by detecting changes in the leaf water content [63], the early vegetative stage is composed of smaller leaf portions relative to the bare soil [64], therefore affecting the performance of the index. Overall, our results indicate that low canopy coverage in the V5 stage was impacted by soil background reflectance during image acquisition; thus, the RedEdge and NIR bands led to the highest RMSE achieved and the poor performance of CWSI prediction.

The lowest RMSE of 0.03 was attained when predicting the CWSI during the middle vegetative stage (V10) using the Red band, TIR band, GNDVI, TCARI, CI_Green, and CCCI as the best variables, in order of significance. Meanwhile, the late vegetative stage (V14) yielded an RMSE of 0.05 using NDRE, MTCI, CCCI, GNDVI, TIR band, CI_RedEdge, MTVI2, and Red band as the best variables, in order of significance. Generally, the late vegetative stages are characterized by high LAI and stronger chlorophyll concentrations, which are sensitive to these spectral derivatives [65]. In addition, the high levels of chlorophyll, due to maize reaching photosynthetic maturity and requiring a high degree of productivity for fruit production, are associated with later vegetative stages [32]. Our results reveal that the chlorophyll-based VIs and bands (such as the Red band, CI_Green, CCCI, CI_RedEdge) were significant to the estimation of the CWSI. Perhaps dense canopy coverage, which presents a homogenous scene of green pigment reflectance during image acquisition, led to the optimal prediction of the CWSI in the smallholder field due to little to no soil background disturbance. Comparable findings were observed by [4,66,67], who noted that there was a high chlorophyll concentration in the late vegetative growth stages of maize, which was susceptible to water stress indicators.

During R1, the model prediction resulted in an RMSE of 0.09, with TIR, TCARI, RedEdge, Red, RDVI, RVI, and Green as the best variables, in order of significance. In the 1970s, thermal remote sensing became a possible instrument for detecting early plant water stress [68]. The TIR band has been linked to biophysical parameters such as canopy temperature and stomatal changes resulting from water availability [69]. Plants close their stomata when they experience water stress, thus reducing the loss of water and consequently leading to a reduction in evaporative cooling. This results in a balance between the temperature of the plant's canopy and the surrounding temperature. On the other hand, well-hydrated plants allow transpiration and evaporative cooling to be maintained, which leads to a lower temperature of the canopy [24]. Consequently, it is feasible to identify plant water stress by measuring canopy temperature. The occurrence of water stress in crops can be observed through remote assessments of canopy temperature using thermal infrared (TIR) technology [15,70]. Specifically, canopy temperature, which is strongly determined by TIR, can record released radiant energy [24]. This stage (Maize R1) is characterized by dense canopies, and our results show that the accuracy of estimating the CWSI through the TIR region was improved. Thus, crop surface temperatures were

strongly detected in the reproductive stage (R1) when TIR was the optimal variable for the RF model at this stage.

Overall, previous research has shown that multispectral VIs obtained from UAV data strongly correlate with indicators of water stress, demonstrating the capability to evaluate water stress and its variation through the use of multispectral VIs [25]. Ref. [67] discovered a strong relationship between GNDVI and stomatal conductance. Ref. [71] obtained an R^2 value of 0.68 from a linear regression analysis connecting the NDVI and stem water potential. Ref. [24] reported an R^2 value of 0.77 relating the Photochemical Reflectance Index (PRI) and the CWSI. However, our results indicate that using multispectral VIs and associated bands in the early vegetative stages does not yield optimal results. Similarly, in the early vegetative stages of maize, the highest RMSE was also observed by [32], where they reported the highest RMSE of $13.9 \mu\text{mol}/\text{m}^2$ during the earliest vegetative growth stage of maize when compared with the mid-vegetative as well as the reproductive stages. Even though this is the case, this study indicated that the V10 stage is the most optimal stage, followed by V14, to estimate the CWSI. This suggests the paramount significance of UAV data in maize water stress monitoring, considering that water stress in maize is particularly critical during the tasselling stage since it can lead to significant yield reduction [72].

4.3. Implication of the Findings

As commercial agricultural practices become a focal point of modern innovation and development, smallholder farmers often do not have the necessary resources needed to adopt effective agricultural practices and optimize agricultural production. Therefore, the findings from this study suggest a potential advantage for UAVs, as they may be capable of profoundly investigating near real-time crop water stress detection using the CWSI as a proxy, incorporating multispectral and thermal imaging technology. Therefore, the findings from this study are valuable as a source of information about agricultural water management of smallholder farmers since they provide information about water stress levels at various phenological stages (V5, V10, V14, R1). Notably, the results from this research revealed stages that have a generally low CWSI, with stage V14 showing the highest CWSI level of 0.44, which indicates a slight moisture deficit and, therefore, suggests irrigation intervention during this stage. Irrigating during the vegetative growth phases helps ensure maximum productivity and reduces the risk of early water stress in crops.

The results also suggest the need for the potential adoption of climate-smart practices during the stages that are susceptible to water stress in order to improve crop production and yield. Notably, the UAV data revealed optimal periods for CWSI prediction, particularly during the V10 stage. The effective determination of crop water stress during this vegetative stage is critical since it notably affects crop development as well as productivity. Implementing water management climate-smart practices during this stage could help smallholder farmers achieve desired yields and prevent crop loss.

5. Conclusions

This study sought to identify the optimal phenological stage for predicting the CWSI of maize using UAV data. Based on the results of this research, it can be concluded that data acquired from UAVs can effectively assess water stress in maize during various phenological stages. Data from the UAV resulted in high prediction accuracies in the investigated periods (i.e., V10, V14, and R1). Additionally, the findings reveal that RF regression, when applied to UAV remotely sensed data, can effectively predict the maize CWSI during both the vegetative and reproductive growing stages. To be precise, our main conclusions are as follows:

- The RF regression model demonstrated high predictive accuracies for the CWSI in the investigated maize growth stages, i.e., V10, V14, and R1, with the NDWI, Red band, NDRE, and thermal band being the most influential variables in all the stages, respectively ($R^2 > 0.80$ and $RMSE \leq 0.1$ for all stages).
- The optimal RF model was identified at the V10 growth stage, with the Red band being the most influential variable, followed by the thermal band ($R^2 = 0.85$ and $RMSE = 0.028$).

The Red, RedEdge, NIR, and TIR UAV bands and their associated indices (NDWI, MTCI, GNDVI, NDRE) were significant in the predictors of the CWSI. In addition to identifying stage V10 as the optimal stage, this research also revealed the practicality of assessing maize water stress and monitoring its spatial variability at a farm level through the UAV-based multispectral VI and band regression models developed in this study. The successful quantification of the CWSI using UAV technology provides valuable information for smallholder farmers, enabling them to take precautionary measures and make informed decisions regarding farm management. This positions the technology of UAVs as a credible and promising remote sensing data acquisition tool for precision farming.

Author Contributions: Conceptualization, M.K. and M.S.; methodology, M.K., M.S., L.N. and J.M.; validation, T.M. and S.M.; formal analysis, M.K., M.S., L.N., J.M., S.M. and T.M.; investigation, M.K., M.S., L.N. and J.M.; resources, M.K. and M.S.; data curation, M.K., L.N., J.M. and M.S.; writing—original draft preparation, M.K., M.S., L.N. and J.M.; writing—review and editing, T.M. and S.M.; visualization, T.M.; supervision, S.M.; project administration, T.M.; funding acquisition, M.S. All authors have read and agreed to the published version of the manuscript.

Funding: The Water Research Commission funded this research, Grant Number K5/2971/the Water Research Commission funded four and the APC.

Data Availability Statement: The raw data supporting the conclusions of this article will be made available by the authors on request.

Conflicts of Interest: The authors declare no conflicts of interest.

References

1. Nhamo, L.; Mabhaudhi, T.; Modi, A. Preparedness or repeated short-term relief aid? Building drought resilience through early warning in southern Africa. *Water SA* **2019**, *45*, 75–85. [[CrossRef](#)]
2. Ubisi, N.R.; Mafongoya, P.L.; Kolanisi, U.; Jiri, O. Smallholder farmer's perceived effects of climate change on crop production and household livelihoods in rural Limpopo province, South Africa. *Change Adapt. Socio-Ecol. Syst.* **2017**, *3*, 27–38. [[CrossRef](#)]
3. Sah, R.P.; Chakraborty, M.; Prasad, K.; Pandit, M.; Tudu, V.; Chakravarty, M.; Narayan, S.; Rana, M.; Moharana, D. Impact of water deficit stress in maize: Phenology and yield components. *Sci. Rep.* **2020**, *10*, 2944. [[CrossRef](#)] [[PubMed](#)]
4. Chivasa, W.; Mutanga, O.; Biradar, C. Application of remote sensing in estimating maize grain yield in heterogeneous African agricultural landscapes: A review. *Int. J. Remote Sens.* **2017**, *38*, 6816–6845. [[CrossRef](#)]
5. Zhuang, S.; Wang, P.; Jiang, B.; Li, M.; Gong, Z. Early detection of water stress in maize based on digital images. *Comput. Electron. Agric.* **2017**, *140*, 461–468. [[CrossRef](#)]
6. Steele, D.D.; Stegman, E.C.; Knighton, R.E. Irrigation management for corn in the northern Great Plains, USA. *Irrig. Sci.* **2000**, *19*, 107–114. [[CrossRef](#)]
7. Cakir, R. Effect of water stress at different development stages on vegetative and reproductive growth of corn. *Field Crops Res.* **2004**, *89*, 1–16. [[CrossRef](#)]
8. Li, Y.-H.; Lu, Q.; Wu, B.; Zhu, Y.-J.; Liu, D.-J.; Zhang, J.-X.; JIN, Z.-H. A review of leaf morphology plasticity linked to plant response and adaptation characteristics in arid ecosystems. *Chin. J. Plant Ecol.* **2012**, *36*, 88. [[CrossRef](#)]
9. Idso, S.B.; Jackson, R.D.; Reginato, R.J. Remote-Sensing of Crop Yields: Canopy temperature and albedo measurements have been quantitatively correlated with final harvests of wheat. *Science* **1977**, *196*, 19–25. [[CrossRef](#)]
10. Bazrgar, G.; Kalat, S.M.N.; Khorasani, S.K.; Ghasemi, M.; Kelidari, A. Effect of deficit irrigation on physiological, biochemical, and yield characteristics in three baby corn cultivars (*Zea mays* L.). *Heliyon* **2023**, *9*, e15477. [[CrossRef](#)]

11. Gardner, B.; Blad, B.; Garrity, D.; Watts, D. Relationships between crop temperature, grain yield, evapotranspiration and phenological development in two hybrids of moisture stressed sorghum. *Irrig. Sci.* **1981**, *2*, 213–224. [[CrossRef](#)]
12. Upchurch, D.R.; Wanjura, D.F.; Burke, J.J.; Mahan, J.R. US Department of Agriculture USDA, Biologically-Identified Optimal Temperature Interactive Console (BIOTIC) for Managing Irrigation. U.S. Patent No 5,539,637, 23 July 1996.
13. Nanda, M.K.; Giri, U.; Bera, N. Canopy temperature-based water stress indices: Potential and limitations. In *Advances in Crop Environment Interaction*; Springer: Berlin/Heidelberg, Germany, 2018; pp. 365–385.
14. Gerhards, M.; Schlerf, M.; Rascher, U.; Udelhoven, T.; Juszczak, R.; Alberti, G.; Miglietta, F.; Inoue, Y. Analysis of airborne optical and thermal imagery for detection of water stress symptoms. *Remote Sens.* **2018**, *10*, 1139. [[CrossRef](#)]
15. Jackson, R.D.; Idso, S.; Reginato, R.; Pinter Jr, P. Canopy temperature as a crop water stress indicator. *Water Resour. Res.* **1981**, *17*, 1133–1138. [[CrossRef](#)]
16. Ekinzog, E.K.; Schlerf, M.; Kraft, M.; Werner, F.; Riedel, A.; Rock, G.; Mallick, K. Revisiting crop water stress index based on potato field experiments in Northern Germany. *Agric. Water Manag.* **2022**, *269*, 107664. [[CrossRef](#)]
17. Zhang, L.; Zhang, H.; Niu, Y.; Han, W. Mapping maize water stress based on UAV multispectral remote sensing. *Remote Sens.* **2019**, *11*, 605. [[CrossRef](#)]
18. Yetik, A.K.; Candoğan, B.N. Chlorophyll response to water stress and the potential of using crop water stress index in sugar beet farming. *Sugar Tech* **2023**, *25*, 57–68. [[CrossRef](#)] [[PubMed](#)]
19. Romero-Trigueros, C.; Bayona Gambín, J.M.; Nortes Tortosa, P.A.; Alarcón Cabañero, J.J.; Nicolás Nicolás, E. Determination of crop water stress index by infrared thermometry in grapefruit trees irrigated with saline reclaimed water combined with deficit irrigation. *Remote Sens.* **2019**, *11*, 757. [[CrossRef](#)]
20. Ru, C.; Hu, X.; Wang, W.; Ran, H.; Song, T.; Guo, Y. Evaluation of the crop water stress index as an indicator for the diagnosis of grapevine water deficiency in greenhouses. *Horticulturae* **2020**, *6*, 86. [[CrossRef](#)]
21. Sezen, S.M.; Yazar, A.; Daşgan, Y.; Yücel, S.; Akyıldız, A.; Tekin, S.; Akhoundnejad, Y. Evaluation of crop water stress index (CWSI) for red pepper with drip and furrow irrigation under varying irrigation regimes. *Agric. Water Manag.* **2014**, *143*, 59–70. [[CrossRef](#)]
22. Irmak, S.; Haman, D.Z.; Bastug, R. Determination of crop water stress index for irrigation timing and yield estimation of corn. *Agron. J.* **2000**, *92*, 1221–1227. [[CrossRef](#)]
23. Han, M.; Zhang, H.; DeJonge, K.C.; Comas, L.H.; Gleason, S. Comparison of three crop water stress index models with sap flow measurements in maize. *Agric. Water Manag.* **2018**, *203*, 366–375. [[CrossRef](#)]
24. Zarco-Tejada, P.J.; González-Dugo, V.; Berni, J.A. Fluorescence, temperature and narrow-band indices acquired from a UAV platform for water stress detection using a micro-hyperspectral imager and a thermal camera. *Remote Sens. Environ.* **2012**, *117*, 322–337. [[CrossRef](#)]
25. Zhang, F.; Zhou, G. Estimation of vegetation water content using hyperspectral vegetation indices: A comparison of crop water indicators in response to water stress treatments for summer maize. *BMC Ecol.* **2019**, *19*, 18. [[CrossRef](#)]
26. Gao, S.; Zhong, R.; Yan, K.; Ma, X.; Chen, X.; Pu, J.; Gao, S.; Qi, J.; Yin, G.; Myneni, R.B. Evaluating the saturation effect of vegetation indices in forests using 3D radiative transfer simulations and satellite observations. *Remote Sens. Environ.* **2023**, *295*, 113665. [[CrossRef](#)]
27. Haboudane, D.; Miller, J.R.; Tremblay, N.; Zarco-Tejada, P.J.; Dextraze, L. Integrated narrow-band vegetation indices for prediction of crop chlorophyll content for application to precision agriculture. *Remote Sens. Environ.* **2002**, *81*, 416–426. [[CrossRef](#)]
28. Naidoo, L.; Main, R.; Cho, M.A.; Madonsela, S.; Majazi, N. Machine learning modelling of crop structure within the Maize Triangle of South Africa. *Int. J. Remote Sens.* **2022**, *43*, 27–51. [[CrossRef](#)]
29. Boulesteix, A.L.; Janitza, S.; Kruppa, J.; König, I.R. Overview of random forest methodology and practical guidance with emphasis on computational biology and bioinformatics. *Wiley Interdiscip. Rev. Data Min. Knowl. Discov.* **2012**, *2*, 493–507. [[CrossRef](#)]
30. Magidi, J.; Nhamo, L.; Mpandeli, S.; Mabhaudhi, T. Application of the random forest classifier to map irrigated areas using Google Earth Engine. *Remote Sens.* **2021**, *13*, 876. [[CrossRef](#)]
31. Wang, D.; Gartung, J. Infrared canopy temperature of early-ripening peach trees under postharvest deficit irrigation. *Agric. Water Manag.* **2010**, *97*, 1787–1794. [[CrossRef](#)]
32. Brewer, K.; Clulow, A.; Sibanda, M.; Gokool, S.; Odindi, J.; Mutanga, O.; Naiken, V.; Chimonyo, V.G.; Mabhaudhi, T. Estimation of maize foliar temperature and stomatal conductance as indicators of water stress based on optical and thermal imagery acquired using an unmanned aerial vehicle (UAV) platform. *Drones* **2022**, *6*, 169. [[CrossRef](#)]
33. Rodriguez-Galiano, V.F.; Ghimire, B.; Rogan, J.; Chica-Olmo, M.; Rigol-Sanchez, J.P. An assessment of the effectiveness of a random forest classifier for land-cover classification. *ISPRS J. Photogramm. Remote Sens.* **2012**, *67*, 93–104. [[CrossRef](#)]
34. Kapari, M.; Sibanda, M.; Magidi, J.; Mabhaudhi, T.; Nhamo, L.; Mpandeli, S. Comparing Machine Learning Algorithms for Estimating the Maize Crop Water Stress Index (CWSI) Using UAV-Acquired Remotely Sensed Data in Smallholder Croplands. *Drones* **2024**, *8*, 61. [[CrossRef](#)]
35. Du Plessis, J. *Maize Production*; Department of Agriculture Pretoria, South Africa: Pretoria, South Africa, 2003; p. 38.

36. Ndlovu, H.S.; Odindi, J.; Sibanda, M.; Mutanga, O.; Clulow, A.; Chimonyo, V.G.; Mabhaudhi, T. A comparative estimation of maize leaf water content using machine learning techniques and unmanned aerial vehicle (UAV)-based proximal and remotely sensed data. *Remote Sens.* **2021**, *13*, 4091. [[CrossRef](#)]
37. Zou, X.; Möttus, M. Sensitivity of common vegetation indices to the canopy structure of field crops. *Remote Sens.* **2017**, *9*, 994. [[CrossRef](#)]
38. Radočaj, D.; Šiljeg, A.; Marinović, R.; Jurišić, M. State of major vegetation indices in precision agriculture studies indexed in Web of Science: A review. *Agriculture* **2023**, *13*, 707. [[CrossRef](#)]
39. Allen, R.G.; Pereira, L.S.; Raes, D.; Smith, M. *FAO Irrigation and Drainage: Crop Evapotranspiration*; Food and Agriculture Organization of the United Nations (FAO): Rome, Italy, 1998; p. e156.
40. Gu, S.; Liao, Q.; Gao, S.; Kang, S.; Du, T.; Ding, R. Crop water stress index as a proxy of phenotyping maize performance under combined water and salt stress. *Remote Sens.* **2021**, *13*, 4710. [[CrossRef](#)]
41. Taghvaeian, S.; Chávez, J.L.; Hansen, N.C. Infrared thermometry to estimate crop water stress index and water use of irrigated maize in Northeastern Colorado. *Remote Sens.* **2012**, *4*, 3619–3637. [[CrossRef](#)]
42. Loggenberg, K.; Strever, A.; Greyling, B.; Poona, N. Modelling water stress in a Shiraz vineyard using hyperspectral imaging and machine learning. *Remote Sens.* **2018**, *10*, 202. [[CrossRef](#)]
43. Wright, M.N.; König, I.R. Splitting on categorical predictors in random forests. *PeerJ* **2019**, *7*, e6339. [[CrossRef](#)]
44. Mutanga, O.; Adam, E.; Cho, M.A. High density biomass estimation for wetland vegetation using WorldView-2 imagery and random forest regression algorithm. *Int. J. Appl. Earth Obs. Geoinf.* **2012**, *18*, 399–406. [[CrossRef](#)]
45. Eugenio, F.C.; Grohs, M.; Venancio, L.P.; Schuh, M.; Bottega, E.L.; Ruoso, R.; Schons, C.; Mallmann, C.L.; Badin, T.L.; Fernandes, P. Estimation of soybean yield from machine learning techniques and multispectral RPAS imagery. *Remote Sens. Appl. Soc. Environ.* **2020**, *20*, 100397. [[CrossRef](#)]
46. Veysi, S.; Naseri, A.A.; Hamzeh, S.; Bartholomeus, H. A satellite based crop water stress index for irrigation scheduling in sugarcane fields. *Agric. Water Manag.* **2017**, *189*, 70–86. [[CrossRef](#)]
47. Zhang, W.; Zhao, X.; Gao, X.; Liang, W.; Li, J.; Zhang, B. Spatially explicit assessment of water scarcity and potential mitigating solutions in a large water-limited basin: The Yellow River basin in China. *Hydrol. Earth Syst. Sci. Discuss.* **2024**, *2024*, 1–36.
48. Peng, X.; Hu, X.; Chen, D.; Zhou, Z.; Guo, Y.; Deng, X.; Zhang, X.; Yu, T. Prediction of grape sap flow in a greenhouse based on random forest and partial least squares models. *Water* **2021**, *13*, 3078. [[CrossRef](#)]
49. Gontia, N.; Tiwari, K. Development of crop water stress index of wheat crop for scheduling irrigation using infrared thermometry. *Agric. Water Manag.* **2008**, *95*, 1144–1152. [[CrossRef](#)]
50. Meiyan, S.; Qizhou, D.; ShuaiPeng, F.; Xiaohong, Y.; Jinyu, Z.; Lei, M.; Baoguo, L.; Yuntao, M. Improved estimation of canopy water status in maize using UAV-based digital and hyperspectral images. *Comput. Electron. Agric.* **2022**, *197*, 106982. [[CrossRef](#)]
51. Berni, J.; Zarco-Tejada, P.; Sepulcre-Cantó, G.; Fereres, E.; Villalobos, F. Mapping canopy conductance and CWSI in olive orchards using high resolution thermal remote sensing imagery. *Remote Sens. Environ.* **2009**, *113*, 2380–2388. [[CrossRef](#)]
52. Bellvert, J.; Marsal, J.; Girona, J.; Gonzalez-Dugo, V.; Fereres, E.; Ustin, S.L.; Zarco-Tejada, P.J. Airborne thermal imagery to detect the seasonal evolution of crop water status in peach, nectarine and Saturn peach orchards. *Remote Sens.* **2016**, *8*, 39. [[CrossRef](#)]
53. Jamshidi, S.; Zand-Parsa, S.; Kamgar-Haghighi, A.A.; Shahsavari, A.R.; Niyogi, D. Evapotranspiration, crop coefficients, and physiological responses of citrus trees in semi-arid climatic conditions. *Agric. Water Manag.* **2020**, *227*, 105838. [[CrossRef](#)]
54. Tanriverdi, C.; Degirmenci, H.; Gonen, E.; Boyacı, S. A comparison of the gravimetric and TDR methods in terms of determining the soil water content of the corn plant. *Sci. Pap. Ser. A Agron.* **2016**, *59*, 153–158.
55. Ihuoma, S.O.; Madramootoo, C.A. Recent advances in crop water stress detection. *Comput. Electron. Agric.* **2017**, *141*, 267–275. [[CrossRef](#)]
56. Sharma, P.K.; Kumar, D.; Srivastava, H.S.; Patel, P. Assessment of different methods for soil moisture estimation: A review. *J. Remote Sens. GIS* **2018**, *9*, 57–73.
57. Kumar, N.; Shankar, V.; Poddar, A. Agro-hydrologic modelling for simulating soil moisture dynamics in the root zone of Potato based on crop coefficient approach under limited climatic data. *ISH J. Hydraul. Eng.* **2022**, *28*, 310–326. [[CrossRef](#)]
58. Wijewardana, C.; Alsajri, F.A.; Irby, J.T.; Krutz, L.J.; Golden, B.; Henry, W.B.; Gao, W.; Reddy, K.R. Physiological assessment of water deficit in soybean using midday leaf water potential and spectral features. *J. Plant Interact.* **2019**, *14*, 533–543. [[CrossRef](#)]
59. Li, Q.; Gao, M.; Li, Z.-L. Ground hyper-spectral remote-sensing monitoring of wheat water stress during different growing stages. *Agronomy* **2022**, *12*, 2267. [[CrossRef](#)]
60. Raper, T.; Varco, J. Canopy-scale wavelength and vegetative index sensitivities to cotton growth parameters and nitrogen status. *Precis. Agric.* **2015**, *16*, 62–76. [[CrossRef](#)]
61. Hallik, L.; Kazantsev, T.; Kuusk, A.; Galmés, J.; Tomás, M.; Niinemets, Ü. Generality of relationships between leaf pigment contents and spectral vegetation indices in Mallorca (Spain). *Reg. Environ. Chang.* **2017**, *17*, 2097–2109. [[CrossRef](#)]

62. Imran, H.A.; Gianelle, D.; Rocchini, D.; Dalponte, M.; Martín, M.P.; Sakowska, K.; Wohlfahrt, G.; Vescovo, L. VIS-NIR, red-edge and NIR-shoulder based normalized vegetation indices response to co-varying leaf and Canopy structural traits in heterogeneous grasslands. *Remote Sens.* **2020**, *12*, 2254. [[CrossRef](#)]
63. Shashikant, V.; Mohamed Shariff, A.R.; Wayayok, A.; Kamal, M.R.; Lee, Y.P.; Takeuchi, W. Utilizing TVDI and NDWI to classify severity of agricultural drought in Chuping, Malaysia. *Agronomy* **2021**, *11*, 1243. [[CrossRef](#)]
64. Wang, C.; He, J.; Zhao, T.-H.; Cao, Y.; Wang, G.; Sun, B.; Yan, X.; Guo, W.; Li, M.-H. The smaller the leaf is, the faster the leaf water loses in a temperate forest. *Front. Plant Sci.* **2019**, *10*, 58. [[CrossRef](#)]
65. Ustin, S.L.; Jacquemoud, S. How the optical properties of leaves modify the absorption and scattering of energy and enhance leaf functionality. *Remote Sens. Plant Biodivers.* **2020**, *110*, 349–384.
66. Xie, C.; Yang, C. A review on plant high-throughput phenotyping traits using UAV-based sensors. *Comput. Electron. Agric.* **2020**, *178*, 105731. [[CrossRef](#)]
67. Zúñiga Espinoza, C.; Khot, L.R.; Sankaran, S.; Jacoby, P.W. High resolution multispectral and thermal remote sensing-based water stress assessment in subsurface irrigated grapevines. *Remote Sens.* **2017**, *9*, 961. [[CrossRef](#)]
68. Gerhards, M.; Schlerf, M.; Mallick, K.; Udelhoven, T. Challenges and future perspectives of multi-/Hyperspectral thermal infrared remote sensing for crop water-stress detection: A review. *Remote Sens.* **2019**, *11*, 1240. [[CrossRef](#)]
69. Poblete-Echeverría, C.; Espinace, D.; Sepúlveda-Reyes, D.; Zúñiga, M.; Sanchez, M. Analysis of crop water stress index (CWSI) for estimating stem water potential in grapevines: Comparison between natural reference and baseline approaches. In Proceedings of the VIII International Symposium on Irrigation of Horticultural Crops 1150, Lleida, Spain, 8–11 June 2015; pp. 189–194.
70. Quemada, C.; Pérez-Escudero, J.M.; Gonzalo, R.; Ederra, I.; Santesteban, L.G.; Torres, N.; Iriarte, J.C. Remote sensing for plant water content monitoring: A review. *Remote Sens.* **2021**, *13*, 2088. [[CrossRef](#)]
71. Baluja, J.; Diago, M.P.; Balda, P.; Zorer, R.; Meggio, F.; Morales, F.; Tardaguila, J. Assessment of vineyard water status variability by thermal and multispectral imagery using an unmanned aerial vehicle (UAV). *Irrig. Sci.* **2012**, *30*, 511–522. [[CrossRef](#)]
72. Pradawet, C.; Khongdee, N.; Pansak, W.; Spreer, W.; Hilger, T.; Cadisch, G. Thermal imaging for assessment of maize water stress and yield prediction under drought conditions. *J. Agron. Crop Sci.* **2023**, *209*, 56–70. [[CrossRef](#)]

Disclaimer/Publisher’s Note: The statements, opinions and data contained in all publications are solely those of the individual author(s) and contributor(s) and not of MDPI and/or the editor(s). MDPI and/or the editor(s) disclaim responsibility for any injury to people or property resulting from any ideas, methods, instructions or products referred to in the content.